

GNC TECHNICAL MEMO

---

<b>Title</b>	Starlink Conjunction Avoidance with Crewed Space Stations
<b>Memo No.</b>	SAT-51385
<b>Author</b>	Starlink GNC Team
<b>Department</b>	GNC
<b>Date</b>	Saturday 23 <sup>rd</sup> April, 2022, 10:33

## Contents

<b>1</b>	<b>Introduction</b>	<b>3</b>
<b>2</b>	<b>Starlink Mission Design</b>	<b>4</b>
2.1	Orbit Parameterization . . . . .	5
2.2	Time-Optimal Orbit Design . . . . .	6
2.3	Deviations from the Time-Optimal Solution . . . . .	8
<b>3</b>	<b>Dynamics Relative to Space Stations</b>	<b>10</b>
3.1	Minimum Clearance . . . . .	11
3.2	Close-Approach Geometry . . . . .	12
3.2.1	Approximation for circular orbits . . . . .	13
3.2.2	High-fidelity operational model . . . . .	13
<b>4</b>	<b>Concept of Operations</b>	<b>15</b>
4.1	Reference Trajectory Deconfliction . . . . .	15
4.2	Prediction Quality and Reactive Re-Planning . . . . .	16
<b>5</b>	<b>Conclusions</b>	<b>18</b>

# 1 Introduction

SpaceX has made space safety one of its top priorities when planning trajectories of Starlink satellites, especially when crossing the orbits of the International Space Station (ISS) and the Chinese Space Station Tiangong. Furthermore, SpaceX is committed to transparently sharing any information that improves the cooperation with the space station operators. As part of this effort, this memorandum describes how Starlink trajectories are designed to avoid conjunctions with the ISS and Tiangong following two guiding principles:

- Prevent the trajectories of Starlink satellites from entering a keepout volume centered at either space station to guarantee the safety of the crew and minimize the impact on the space station’s operations. This includes providing crewed space stations the right of way when planning trajectories so that no avoidance maneuvers are required on their part.
- Implement an equitable approach to all crewed space stations, regardless of national origin.

Section 2 explains how the trajectories of the Starlink satellites are parameterized and presents the time-optimal path-planning algorithm used under nominal conditions. Next, the costs of deviating from the optimal trajectory when the optimal solution is not viable due to, for example, potential conjunctions with either space station are discussed. The motion of Starlink satellites relative to the space stations and SpaceX’s high-fidelity model for predicting conjunctions are described in Section 3. Finally, Section 4 outlines how the trajectories are adjusted to avoid potential conjunctions and how the operations team monitors and reacts to potential conjunctions.

The techniques for avoiding conjunctions at the planning stages presented here are an additional precaution in addition to Starlink’s collision-avoidance system. In this context, conjunction avoidance during planning refers to designing trajectories that maintain satellites far away from space stations under nominal circumstances. Deconflicting trajectories at the planning stage requires predicting potential conjunctions several weeks into the future, which naturally limits the accuracy of the results. As part of SpaceX’s multi-tiered approach to space safety, Starlink’s automatic collision avoidance system allows satellites to plan maneuvers to minimize the collision probability during close approaches that could not be avoided when planning.

## Nomenclature

$a$	Semimajor axis, m	$\Delta r^*$	Radial offset at the plane crossings, m
$e$	Eccentricity	$\epsilon_{\Omega}$	RAAN error, rad
$f$	True anomaly, rad	$\theta$	Along-track angle, rad
$h$	Semimajor axis altitude, m	$\dot{\theta}$	Along-track rate, rad/s
$i$	Orbital inclination, rad	$\ddot{\theta}$	Along-track acceleration, rad/s <sup>2</sup>
$M$	Mean anomaly, rad	$\psi$	Conjunction anomaly, rad
$n$	Mean motion, rad/s	$\omega$	Argument of perigee, rad
$r$	Orbital radius, m	$\Omega$	Right ascension of the ascending node (RAAN), rad
$t$	Time, s	$\dot{\Omega}$	RAAN rate, rad/s
$T_s$	Synodic period, s		
$u$	Argument of latitude, rad		

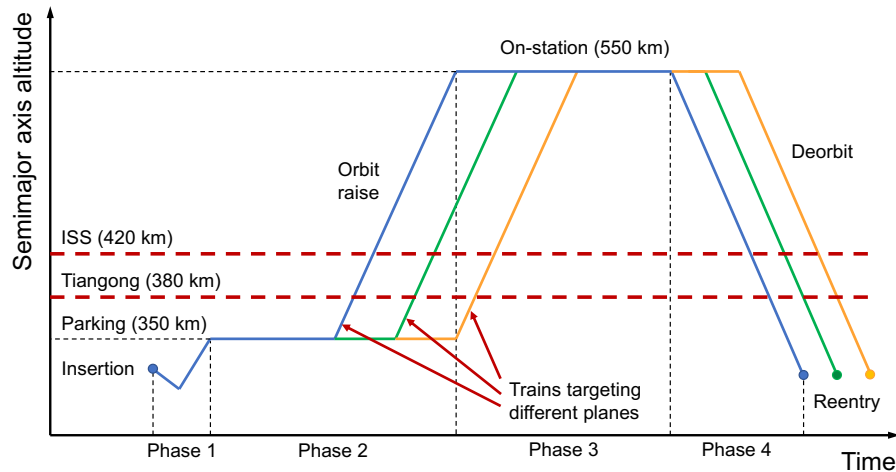


**Figure 2.1:** Typical mission profile of Starlink satellites.

## 2 Starlink Mission Design

The Starlink constellation consists of several orbital shells in the 500–600 km altitude range, each comprising up to 72 orbital planes. Each orbital plane can host multiple satellites in prescribed orbital slots. When planning the trajectory of a satellite targeting a specific on-station slot, the goal is to minimize the time it takes for the satellite to arrive at its destination and start serving customers. Minimizing the time-to-station presents several advantages:

- Reduces the time it takes for a satellite to start serving customers.
- Maximizes the lifetime of the satellite by minimizing the time spent at lower altitudes where the propellant required to counteract atmospheric drag is highest.

Typical Starlink trajectory profiles consist of four phases:

1. Orbit insertion followed by a ballistic segment and orbit raise to a parking orbit with an altitude generally between 350 km and 360 km.
2. Orbit raise from parking to predefined slots in orbital shells at the service altitudes.
3. Station-keeping and nominal operations at the service altitude.
4. At the end of their operational life, deorbit the satellites in a controlled manner below an altitude threshold for a safe and controlled atmospheric reentry.

Figure 2.1 sketches the different mission phases listed above. The satellites' insertion orbit varies, with perigee altitude as low as 208 km and apogee altitude as high as 340 km, but are generally fully below ISS and Tiangong. SpaceX prefers a low insertion orbit for three reasons: (1) it maximizes the number of satellites delivered to orbit, reducing costs, (2) it tests the ability of the satellites to control their attitude at low altitudes to ensure they will remain controllable during the disposal phase, and (3) in the rare event that any satellites are dead or non-maneuverable at insertion, the high drag environment results in their quick decay and demise. In contrast, launching satellites directly above the crewed space stations means any dead-on-arrival satellites will eventually decay through the stations' orbits in an uncontrolled fashion posing significantly more risk.

Each Starlink launch typically includes enough satellites to fill several orbital planes. For this reason, a train of satellites is usually divided into smaller trains that depart from parking on different dates to target specific orbital planes.

## 2.1 Orbit Parameterization

Starlink satellites plan maneuvers autonomously to follow prescribed reference trajectories. The reference trajectories are modeled using mean orbital elements (Brouwer, 1959), whose evolution is driven by the  $J_2$  component of Earth's gravity field. When averaged over one orbit ignoring maneuvers and drag, the resulting mean semimajor axis, eccentricity, and inclination remain constant over time while the right-ascension of the ascending node (RAAN) undergoes a secular evolution with a constant rate:

$$\dot{\Omega} = -\frac{3nR_{\oplus}^2 J_2}{2a^2(1-e^2)^2} \cos i \quad (2.1.1)$$

where  $n = \sqrt{\mu/a^3}$  is the mean motion and  $R_{\oplus}$  is Earth's equatorial radius. Table 2.1 defines the physical constants. Note that the resulting precession of the line of nodes is retrograde (clock-wise when looking North to South) for prograde orbits ( $i < \pi/2$ ), whereas the nodal precession is prograde (counter-clock-wise) for retrograde orbits ( $i > \pi/2$ ). Furthermore, the RAAN rate is inversely proportional to the semimajor axis.

**Table 2.1:** Physical constants.

Constant	Value	Units	Description
$J_2$	0.0010826298	–	Earth's degree-two zonal harmonic
$R_{\oplus}$	6378137	m	Earth's equatorial radius
$\mu$	$3.986 \times 10^{14}$	$\text{m}^3/\text{s}^2$	Earth's gravitational parameter

The mean eccentricity is chosen so that the orbit is *frozen* in eccentricity and argument of perigee (Coffey et al., 1994). The osculating argument of perigee oscillates around a constant mean argument of perigee equal to  $\pi/2$ . The frozen orbit configuration is stable ensuring that small deviations do not result in the argument of perigee rotating around the orbit and sweeping the entire range from 0 to  $2\pi$ .

The evolution of the satellites on their reference trajectories is given by the along-track angle

$$\theta = M + \omega \quad (2.1.2)$$

The  $J_2$ -driven nodal period can be characterized with the along-track rate  $\dot{\theta}$  (Vallado, 1997, §9.6):

$$\dot{\theta} = n + J_2 g(a, e, i) \quad (2.1.3)$$

just like the Keplerian orbital period relates to the mean motion. Both the mean motion  $n$  and the perturbation function  $g$  are inversely proportional to the semimajor axis.

Starlink satellites carry low-thrust electric propulsion systems and the thrust during the orbit-raising and orbit-lowering segments is modeled with a constant along-track acceleration

$$\ddot{\theta} = \text{const.} \quad (2.1.4)$$

The contribution of  $J_2$  to the along-track rate can be neglected when converting the along-track acceleration to the rate of change of the semimajor axis resulting in:

$$\ddot{\theta} \approx -\frac{3n}{2a} \frac{da}{dt} \quad (2.1.5)$$

The rate of change of the semimajor axis is approximately constant over the range of altitudes where Starlink satellites operate:

$$\dot{a} = \frac{da}{dt} \approx \text{const.} \quad (2.1.6)$$

The maximum raise rate that a satellite can sustain is a function of the power harvested and floor power required during orbit transfer and the solar geometry, among other factors. The maximum achievable rate of change of the semimajor axis also depends on the drag acceleration experienced by the vehicle. When orbit raising ( $\dot{a} > 0$ ), drag opposes the thrust acceleration and reduces the net raise rate achieved by the thruster. When orbit lowering ( $\dot{a} < 0$ ), drag contributes to increasing the magnitude of  $\dot{a}$ .

## 2.2 Time-Optimal Orbit Design

From the four mission phases outlined in Section 2, only phases 2 and 4 are relevant for crewed-station deconfliction. The trajectory profile in either case reduces to a station-keeping segment followed by an orbit-raising (park-to-station) or orbit-lowering (deorbit) segment. For conciseness, the analysis that follows mostly focuses on satellites raising from parking to their target service orbit. Deorbit trajectories are produced in the same way by reversing the altitude profiles and relaxing the terminal constraints on arrival RAAN and along-track angle.

When targeting the along-track rate of the destination orbit  $\dot{\theta}_{\text{tgt}}$  (equivalent to targeting a specific semimajor axis) given a constant along-track acceleration, the required transfer time reduces to

$$\Delta t_t = \frac{\dot{\theta}_{\text{tgt}} - \dot{\theta}_p}{\ddot{\theta}} \quad (2.2.1)$$

where  $\dot{\theta}_p$  denotes the along-track rate on the parking orbit. The difference between the along-track rate at the target orbit and the parking orbit defines the synodic period

$$T_s = \frac{2\pi}{\dot{\theta}_p - \dot{\theta}_{\text{tgt}}} \quad (2.2.2)$$

which is the time it takes to complete one relative orbit. Using the example values in Table 2.2, the transfer time is 43 days and the synodic period between the parking and destination orbits is 1.5 days.

**Table 2.2:** Representative orbital parameters of Starlink satellites.

Variable	Value	Units	Description
$h_p$	350	km	Mean semimajor axis altitude of the parking orbit
$h_{\text{tgt}}$	550	km	Mean semimajor axis altitude of the service orbit
$h_w$	420	km	Mean semimajor axis altitude of the waypoint orbit
$h_r$	560	km	Mean semimajor axis altitude of the reverse-precession orbit
$\dot{a}$	4.7	km/day	Semimajor axis raise rate
$e$	0.001	–	Mean eccentricity
$i$	53	deg	Mean orbital inclination

The raise rate should ideally be as high as possible to minimize the transfer time. On the other hand, if the raise rate is too high, raising satellites may be unable to sustain the burn duration and frequency required to follow their reference trajectories. A representative value of  $\dot{a} = 4.7$  km/day is chosen for this memorandum based on the power available to the propulsion system during worst-case solar geometries and typical drag profiles.

Consider a satellite trajectory raising from parking to station (phase 2 in Fig. 2.1). Once the constant along-track acceleration is known, the transfer time follows from Eq. (2.2.1). Based on the parameterization described in Section 2.1, there is only one degree of freedom left for planning: the take-off time when the satellite initiates the raise.

The design of a time-optimal trajectory reduces to finding the earliest take-off time subject to terminal constraints on the RAAN and along-track angle at the arrival time  $t_f$ . The target values of RAAN,  $\Omega_{\text{tgt}}$ , and along-track angle,  $\theta_{\text{tgt}}$ , depend on the specific slot that each satellite is targeting in the constellation. The constraints on the arrival along-track angle and RAAN take the form:

$$\theta(t_f) - \theta_{\text{tgt}}(t_f) = 2N\pi \quad (2.2.3)$$

$$\Omega(t_f) - \Omega_{\text{tgt}}(t_f) = 0 \quad (2.2.4)$$

Since there is only one degree of freedom (the take-off time,  $t_d$ ) and two constraints (Eqs. 2.2.3 and 2.2.4) the problem is over constrained and generally both constraints cannot be satisfied simultaneously. The number of revolutions  $N > 0$  is also a free parameter but it cannot be used to enforce a second constraint exactly because it can only take integer values. Still, the value of  $N$  can be chosen to minimize the constraint errors. Note that Eq. (2.2.4) does not generally benefit from increasing the number of RAAN revolutions.

Equation (2.2.3) can be solved for the take-off time that satisfies the along-track constraint,

$$t_{d,\theta} = t_0 + \Delta t_{d,\theta} + NT_s \quad \text{with} \quad \Delta t_{d,\theta} = \text{mod} \left( \frac{\Delta\theta_p - \Delta\theta_t}{\dot{\theta}_p - \dot{\theta}_{\text{tgt}}}, T_s \right) \quad (2.2.5)$$

The term  $\Delta\theta_p = \theta_{\text{tgt}}(t_0) - \theta_p(t_0)$  is the relative along-track angle evaluated at the reference epoch  $t_0$ ,  $\Delta\theta_t = \Delta t_i(\dot{\theta}_p - \dot{\theta}_{\text{tgt}})/2$  is the relative along-track angle accumulated during the raising segment, and mod represents the modulo operator. Similarly, the departure time that satisfies Eq. (2.2.4) can be written as

$$t_{d,\Omega} = t_0 + \frac{\Delta\Omega_p - \Delta\Omega_t}{\dot{\Omega}_p - \dot{\Omega}_{\text{tgt}}} \quad (2.2.6)$$

in terms of the relative RAAN precessed during the transfer,  $\Delta\Omega_t$ , and the relative RAAN at the parking orbit  $\Delta\Omega_p = \Omega_{\text{tgt}}(t_0) - \Omega_p(t_0)$ . The angular difference in Eq. (2.2.6) should be wrapped appropriately to ensure  $t_{d,\Omega}$  occurs in the future. To minimize the RAAN error while satisfying the along-track constraint, the number of revolutions  $N$  is obtained by rounding the difference between both solutions to the nearest integer number of synodic periods

$$N = \left\lceil \frac{t_{d,\Omega} - t_0 - \Delta t_{d,\theta}}{T_s} \right\rceil \quad (2.2.7)$$

This value of  $N$  is then used to compute the take-off time from Eq. (2.2.5). The maximum RAAN error resulting from this approach is given by the precession over half of a synodic period

$$\varepsilon_{\Omega,\text{max}} = \frac{T_s}{2} |\dot{\Omega}_p - \dot{\Omega}_{\text{tgt}}| \quad (2.2.8)$$

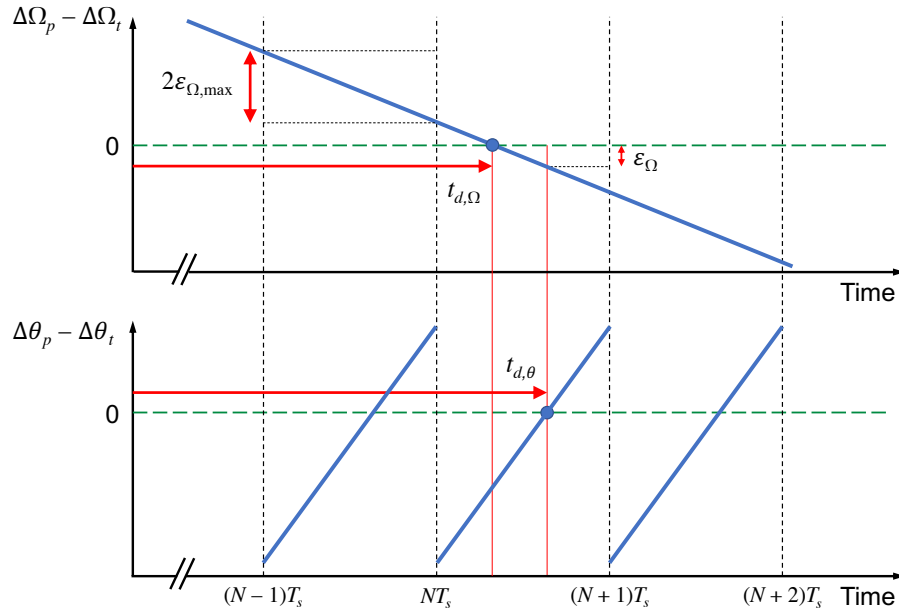


**Figure 2.2:** Schematic representation of the RAAN constraint (top) and the along-track constraint (bottom).

which amounts to  $0.36^\circ$  for the example in Table 2.2. The unavoidable RAAN error can be corrected with a propulsive RAAN-offset rate during orbit raise that is, at most,

$$\Delta\dot{\Omega}_\epsilon = \frac{\epsilon_{\Omega,\max}}{\Delta t_t} \tag{2.2.9}$$

Figure 2.2 is a graphical representation of the constraints in Eqs. (2.2.4) and (2.2.3). The top panel shows the time evolution of the RAAN error and the bottom panel shows the evolution of the along-track error. The RAAN error profile crosses zero after  $N$  revolutions and the difference  $t_{d,\Omega} - t_{d,\theta}$  determines the final error in the RAAN constraint,  $\epsilon_\Omega$ , which is bounded by  $|\epsilon_\Omega| \leq \epsilon_{\Omega,\max}$ . Solutions that satisfy the along-track constraint in Eq. (2.2.3) can be found on every synodic revolution.

The difference in optimal take-off times when targeting two consecutive orbital planes in the constellation is approximately

$$\Delta t_{\text{planes}} = \frac{2\pi/N_{\text{planes}}}{|\dot{\Omega}_p - \dot{\Omega}_{\text{tgt}}|} \tag{2.2.10}$$

For shells with 72 orbital planes and the orbital parameters in Table 2.2, the take-off times of satellites targeting contiguous planes are approximately 10 days apart.

### 2.3 Deviations from the Time-Optimal Solution

If a satellite cannot depart at its time-optimal take-off time, it incurs larger RAAN errors. The new take-off time  $t'_d$  is defined in terms of a time offset  $\Delta t_d$  relative to the time-optimal take-off time:

$$t'_d = t_d + \Delta t_d \tag{2.3.1}$$

With this notation,  $\Delta t_d < 0$  indicates that the satellite departs early and  $\Delta t_d > 0$  that the satellite departs late. The difference in the amount of RAAN precessed at the parking orbit when departing at  $t'_d$  instead of at  $t_d$  is:

$$\Delta\Omega'_p = (\dot{\Omega}_p - \dot{\Omega}_{\text{tgt}})\Delta t_d \tag{2.3.2}$$

For the case in Table 2.2, the RAAN error accumulates at a rate of  $0.5^\circ$  for every day the departure date is advanced or delayed.

Correcting such RAAN errors with cross-track control can significantly impact the propellant budget of the satellites. Alternatively, the RAAN error can be corrected by sending the satellite to station keep at an intermediate altitude, called a *waypoint* altitude, to continue to precess and compensate for  $\Delta\Omega'_p$ . The time that the satellite must spend at the waypoint to meet the constraint in Eq. (2.2.4) is

$$\Delta t_{w,\Omega} = -\Delta t_d \left( \frac{\dot{\Omega}_p - \dot{\Omega}_{\text{tgt}}}{\dot{\Omega}_w - \dot{\Omega}_{\text{tgt}}} \right) \quad (2.3.3)$$

where  $\dot{\Omega}_w$  denotes the RAAN rate at the waypoint altitude. As discussed in Section 2.2, a second constraint must also be enforced to make sure that the satellite arrives at its target along-track angle (Eq. 2.2.3). The required time at the waypoint altitude from an along-track angle perspective is

$$\Delta t_{w,\theta} = -\Delta t_d \left( \frac{\dot{\theta}_p - \dot{\theta}_{\text{tgt}}}{\dot{\theta}_w - \dot{\theta}_{\text{tgt}}} \right) \quad (2.3.4)$$

Equations (2.3.3) and (2.3.4) must hold simultaneously to satisfy the boundary conditions. Even though the problem is over constrained and both conditions cannot be met exactly at the same time, the difference between the relative RAAN-rate ratio and the relative along-track-rate ratio is small over the Starlink altitudes. Therefore, the waypoint duration is chosen to satisfy the along-track constraint following Eq. (2.3.4):

$$\frac{\dot{\Omega}_p - \dot{\Omega}_{\text{tgt}}}{\dot{\Omega}_w - \dot{\Omega}_{\text{tgt}}} \approx \frac{\dot{\theta}_p - \dot{\theta}_{\text{tgt}}}{\dot{\theta}_w - \dot{\theta}_{\text{tgt}}} \implies \Delta t_{w,\Omega} \approx \Delta t_{w,\theta} = \Delta t_w \quad (2.3.5)$$

and any residual RAAN error can be corrected with propulsive maneuvers, if necessary.

Both Eq. (2.3.3) and (2.3.4) must yield positive waypoint durations, which constrains the waypoint altitude (recalling that the magnitudes of both the RAAN rate and the along-track rate are inversely proportional to the semimajor axis) based on the sign of  $\Delta t_d$ :

**Departing early** ( $\Delta t_d < 0$ ): the corresponding relative-rate ratio must be positive. This condition forces the waypoint to be *below* the destination orbit ( $\dot{\theta}_w > \dot{\theta}_{\text{tgt}}$ ), just like the parking orbit.

**Departing late** ( $\Delta t_d > 0$ ): the corresponding relative-rate ratio must be negative. This condition forces the waypoint to be *above* the destination orbit ( $\dot{\theta}_w < \dot{\theta}_{\text{tgt}}$ ), resulting in reverse precession to precess back into the target plane.

Figure 2.3 depicts the relative RAAN and semimajor axis profiles for three different scenarios. Case 1 (blue) corresponds to the time-optimal profile that takes off from parking as soon as it accumulates enough precession to reach the destination RAAN at the end of the raising segment. Case 2 (green) represents a satellite departing early from parking and stopping at a waypoint before arriving to station. Case 3 (red) represents a satellite departing late, which raises above the target orbit to reverse precess and then lowers its orbit back to station.

The total increase in the duration of the transfer is:

$$\Delta t_{\text{tot}} = \Delta t_d + \Delta t_w = \Delta t_d \left( \frac{\dot{\theta}_w - \dot{\theta}_p}{\dot{\theta}_w - \dot{\theta}_{\text{tgt}}} \right) > 0 \quad (2.3.6)$$

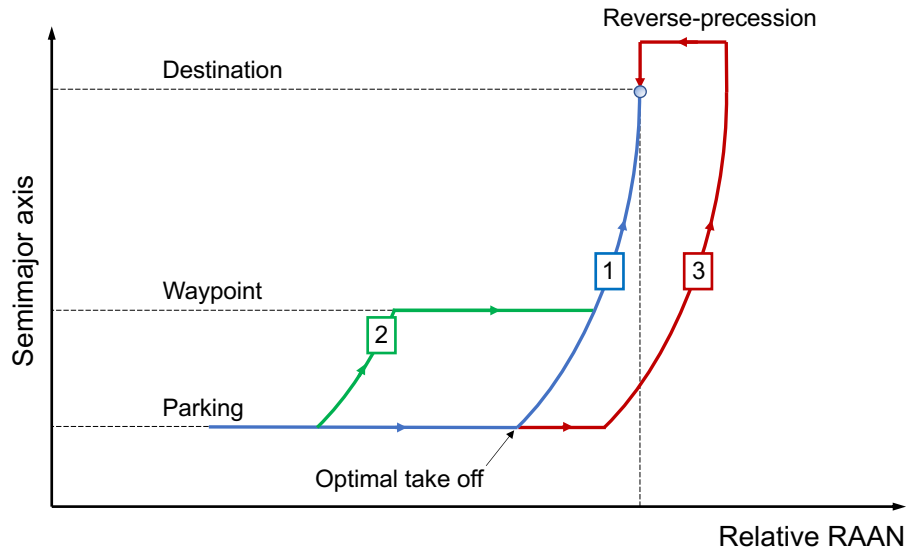


**Figure 2.3:** Schematic representation of typical precession profiles for three different mission scenarios.

It is always positive based on the constraint on the waypoint altitude given the sign of  $\Delta t_d$ . The waypoint altitude should be as low as possible to minimize the increase in the mission duration, which exposes the two main disadvantages of departing late compared to departing early:

1. The required duration of a waypoint above the destination orbit is substantially longer than the duration of a waypoint close to the parking orbit for the same change in departure time, usually about 20 or 30 times longer. As an example using the values in Table 2.2,  $\Delta t_{\text{tot}} = 0.6|\Delta t_d|$  for a waypoint at 420 km ( $\Delta t_d < 0$ ) and  $\Delta t_{\text{tot}} = 22\Delta t_d$  for a waypoint at 560 km ( $\Delta t_d > 0$ ).
2. The satellite burns additional propellant to raise above the target orbit just to lower its orbit again after reverse precessing. In the reference example, approximately 10% of the propellant required to raise to station is spent in this phase.

For these reasons, departing early is preferred over departing late when the satellites cannot take off at the time-optimal time.

### 3 Dynamics Relative to Space Stations

To ensure that the reference trajectories of Starlink satellites do not conflict with the space stations, the first step is to model the relative dynamics between the two. Figure 3.1 depicts the orbits of a space station and a hypothetical Starlink satellite and highlights relevant angles that will be described in this section. The dynamics relative to the space station are usually formulated in the radial-transverse-normal (RTN) frame: the  $x$ -axis is parallel to the station's radius vector (R), the  $z$ -axis is normal to the orbital plane (N), and the  $y$ -axis completes a dextral orthogonal reference frame (T).

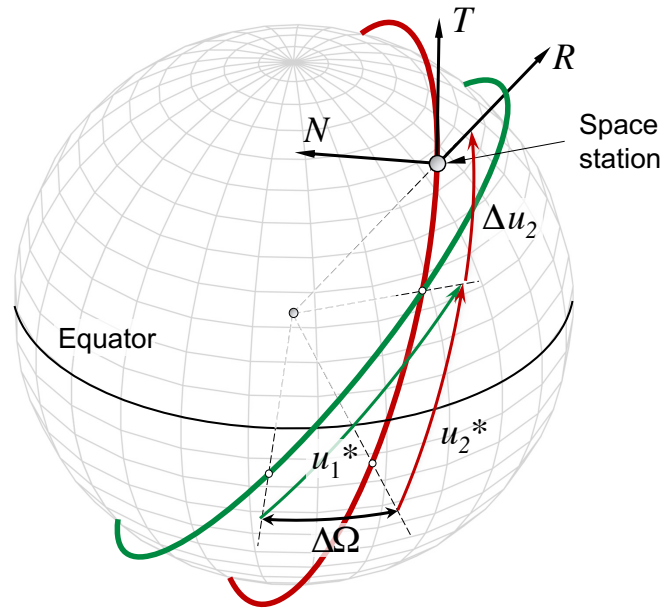


Figure 3.1: Relative orbital geometry and definition of the RTN frame centered at the space station.

In this section, Starlink satellites are the primary objects (1) and a space station the secondary object (2). Table 3.3 presents reference values to support the analysis in the sections that follow.

Table 3.3: Representative orbital parameters of a space station.

Variable	Value	Units	Description
$h$	380	km	Mean semimajor axis altitude
$e$	0.0008	–	Mean eccentricity
$i$	41.5	deg	Mean orbital inclination

### 3.1 Minimum Clearance

Starlink reference trajectories are designed to never intersect a keepout volume centered at the space stations. This keepout volume is modeled as an ellipsoid in the RTN frame. SpaceX chooses

$$R_{\min} = \pm 5 \text{ km}, \quad T_{\min} = \pm 1000 \text{ km}, \quad N_{\min} = \pm 40 \text{ km} \quad (3.1.1)$$

to define the extent of the ellipsoid in the radial, transverse, and normal directions, which ensures Starlink satellites remain outside of typical conjunction screening volumes (18th SPCS, 2020). Safety is the main driver when establishing the dimensions of the ellipsoid and substantial margins are added on top of these values at the planning stage as an additional protection against ephemeris uncertainties and other unforeseen effects (several kilometers to  $R_{\min}$ ,  $N_{\min}$  and hundreds of kilometers to  $T_{\min}$ ). The transverse dimension of the keepout is substantially larger than the radial and normal because the transverse direction is most sensitive to the uncertainty in position and velocity of the space station.

## 3.2 Close-Approach Geometry

Denoting  $[R, T, N]$  the components of the relative position vector of the Starlink satellite relative to the space station in the RTN frame, the condition for a reference trajectory to not intersect the ellipsoidal keepout around the space station is

$$\left(\frac{R}{R_{\min}}\right)^2 + \left(\frac{T}{T_{\min}}\right)^2 + \left(\frac{N}{N_{\min}}\right)^2 > 1 \quad (3.2.1)$$

When the orbits of the satellite and the space station have different inclinations or different RAAN, the normal component  $N$  is large throughout the orbit except close to the two points where the orbits intersect each other's orbital plane (see Fig. 3.1). Therefore, close approaches can only take place at the plane crossings. The contribution from the normal component can be ignored by analyzing the geometry in the vicinity of these points, effectively reducing the dimension of the problem to only the  $(R, T)$  radial-transverse plane.

The argument of latitude

$$u = f + \omega \quad (3.2.2)$$

is used to define the angular position of a spacecraft relative to the equatorial plane measured along its orbit, and  $u_1^*$  and  $u_2^*$  denote the argument of latitude of the points where the primary and secondary orbits intersect the orbital plane of the other orbit, respectively, as sketched in Fig. 3.1. The argument of latitude relative to the intersection point for each spacecraft is

$$\Delta u_i = u_i - u_i^* \quad (3.2.3)$$

The conjunction anomaly

$$\psi = \Delta u_1 - \Delta u_2 = (u_1 - u_2) - (u_1^* - u_2^*) \quad (3.2.4)$$

naturally captures the angular separation between the spacecraft when either of them is at the plane crossing. The difference in argument of latitude at the plane crossing reads:

$$u_1^* - u_2^* = -\arctan \left[ \frac{\sin \Delta\Omega (\cos i_1 + \cos i_2)}{\cos \Delta\Omega (1 + \cos i_1 \cos i_2) + \sin i_1 \sin i_2} \right] \quad (3.2.5)$$

with  $\Delta\Omega = \Omega_1 - \Omega_2$ .

The transverse separation at the plane crossing can be approximated with

$$T \approx a\psi \quad (3.2.6)$$

indicating that  $\psi \rightarrow 0$  is a necessary condition for a close approach.

Finally, the separation in the radial direction at the plane crossing can be approximated with the difference between the orbital radii at those points:

$$R \approx \Delta r^* = r_1^* - r_2^* \quad (3.2.7)$$

The condition for a safe crossing defined in Eq. (3.2.1) transforms into

$$\left(\frac{\Delta r^*}{\Delta r_{\min}}\right)^2 + \left(\frac{\psi}{\psi_{\min}}\right)^2 > 1 \quad (3.2.8)$$

when transcribed to the  $(\psi, \Delta r^*)$  plane.

### 3.2.1 Approximation for circular orbits

When the eccentricity is small for both orbits ( $e_1 \sim e_2 \ll 1$ ), the argument of latitude can be approximated with the along-track angle and the radial offset with the difference between their mean semimajor axes:

$$u \approx \theta, \quad \Delta r^* \approx \Delta a, \quad \psi \approx \theta_1 - \theta_2 - \Delta\theta^* \quad (3.2.9)$$

Under this assumption, the time evolution of the conjunction anomaly and the relative semimajor axis takes the form

$$\psi = \psi_0 + \Delta\dot{\theta}_0 t + \frac{\ddot{\theta}}{2} t^2 \quad (3.2.10)$$

$$\Delta a = \dot{a} t \quad (3.2.11)$$

assuming that  $a_1 = a_2$  at  $t = 0$  and that the mean semimajor axis of the station's orbit remains constant over time. The relative along-track rate at the initial time is  $\Delta\dot{\theta}_0 = \dot{\theta}_{0,1} - \dot{\theta}_{0,2}$ , and  $\ddot{\theta}$  and  $\dot{a}$  are assumed constant. Note that these equations define a parametric parabola in the  $(\psi, \Delta a)$  plane. The vertex of the parabola is reached at  $t = -\Delta\dot{\theta}_0/\ddot{\theta}$ , when the along-track rates coincide. The vertex corresponds to the point where the relative along-track rate flips its sign; the primary spacecraft drifts forward (towards positive  $\psi$ ) relative to the secondary when  $\dot{\theta}_1 > \dot{\theta}_2$ , and backward (towards negative  $\psi$ ) when  $\dot{\theta}_1 < \dot{\theta}_2$ .

For orbits with similar inclinations and eccentricities, Eq. (2.1.3) indicates that the orbits reach the same along-track rate approximately when  $\Delta a = 0$ . In this case, it is  $\Delta\dot{\theta}_0 = 0$  and the value of  $\Delta a$  when the satellites reach the plane crossing ( $\psi = 0$ ),

$$\Delta a_{\psi=0} = \pm \sqrt{\frac{4\dot{a}a\psi_0}{3n}} \quad (3.2.12)$$

can be written as a function of the along-track separation at the  $\Delta a$  intercept,  $a\psi_0$ . The along-track acceleration is converted to the semimajor axis rate of the orbit-transferring Starlink satellite using Eq. (2.1.5).

Figure 3.2 depicts the relative dynamics of orbit-raising and deorbit trajectories on the  $(T, R)$  plane for the same  $\psi_0$  under the simplifications introduced in this section,  $T \approx a\psi$  and  $R \approx \Delta a$ . The figure shows that high raise rates produce larger radial clearances, whereas low raise rates may require larger along-track separations at the radial intercept to stay outside of the keepout.

### 3.2.2 High-fidelity operational model

The simplified model presented in Section 3.2.1 is useful for qualitatively understanding the relative dynamics but the implicit assumptions limit its applicability to real trajectory planning. First, the orbital motion of the space station is subject to atmospheric drag and maneuvers, among other effects, which are not accounted for in Section 3.2.1. These effects can contribute to changing the relative geometry of the encounter by hundreds or even thousands of kilometers.

Second, using the equation of the center (Battin, 1999, p. 212), the orbital radius can be approximated as

$$r = a - ae \cos M + O(e^2) \quad (3.2.13)$$

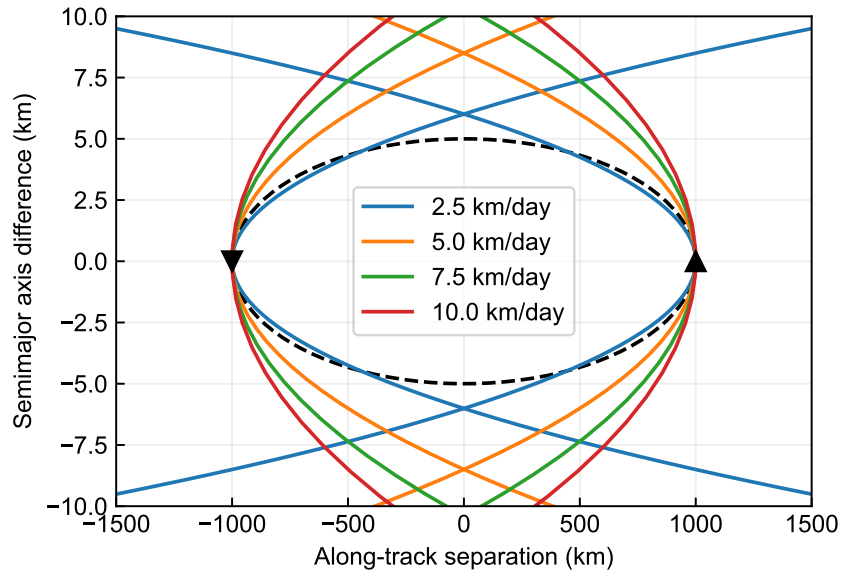


**Figure 3.2:** Schematic representation of Starlink raising and deorbit trajectories relative to a space station for different semi-major axis rates. The dashed ellipsoid represents the keepout and black arrows indicate the direction of motion.

to find that the error in the approximation  $\Delta r^* \approx \Delta a$  can be, to first order, as high as the combined linear eccentricity of both orbits,  $|\Delta r^* - \Delta a| \approx a_1 e_1 + a_2 e_2$ . For the examples in Tables 2.2 and 3.3, the error in the approximation is greater than 12 km, which is more than twice the radial dimension of the keepout.

Third, when the eccentricities and inclinations of the two orbits are not the same, the reversal in along-track rate may not correspond exactly to  $\Delta a = 0$  due to the contribution of the  $J_2$  effects in Eq. (2.1.3). This phenomenon can break the symmetry of the radial miss distance at  $\psi = 0$  obtained in Eq. (3.2.12).

Fourth, the model in Section 3.2.1 does not account for the short and long-period oscillations of the osculating orbital elements due to  $J_2$ . These effects can produce differences between the real and the assumed radial offsets of several kilometers.

For the reasons stated above, SpaceX implements a higher fidelity model to ensure that close encounters are predicted accurately. To estimate the future state of the space station, SpaceX relies on the highest fidelity ephemeris data published by the corresponding operator. Ideally, these predictions include the effects of scheduled maneuvers and other relevant events to avoid discontinuities in the predicted trajectories. When no predictions are published, the latest set of two-line elements (TLEs) for the space station<sup>1</sup> is propagated over time.

To accurately model the radial offset at the plane crossings,  $u^*$ , the osculating orbital radius including the short and long period oscillations induced by Earth’s  $J_2$  is obtained from (Lara, 2015):

$$r_{\text{osc}} = r - \frac{J_2 R_{\oplus}^2}{4p} \left[ (2 - 3s^2) \left( \frac{\kappa}{1 + \eta} + \frac{2\eta}{1 + \kappa} + 1 \right) - s^2 \cos(2u^*) + s^2 \frac{1 - 15c^2}{4(1 - 5c^2)} (\kappa \cos 2u^* + \sigma \sin 2u^*) \right] \quad (3.2.14)$$

where

$$\eta = \sqrt{1 - e^2}, \quad p = a\eta^2, \quad \kappa = \frac{p}{r} - 1, \quad s = \sin i, \quad c = \cos i, \quad \sigma = e \sin f \quad (3.2.15)$$

<sup>1</sup>Retrieved from Space-Track.org.

The osculating radial offset is evaluated at the two plane-crossing points (North and South) to capture the asymmetric nature of the problem.

## 4 Concept of Operations

If the time-optimal reference trajectories of the Starlink satellites described in Section 2.2, which are typically planned weeks in advance, result in potential conflicts with the space station (that is, if they intersect the keepout), they are re-planned to increase the close-approach distance and guarantee a safe crossing.

### 4.1 Reference Trajectory Deconfliction

The relative geometry at the encounter time can be adjusted by changing the take-off time, which is the only degree of freedom available for planning. This is accomplished preferably by departing early rather than late to avoid the higher cost of reverse precession when correcting the RAAN error based on the analysis in Section 2.3.

For typical operational altitudes and inclinations of space stations relative to the Starlink parking orbits, the main effect of departing early by  $\Delta t_d < 0$  is a left-wards shift in the conjunction anomaly at the time of altitude crossing. Conversely, departing late produces a right-wards shift in the  $(\psi, \Delta r^*)$  plane. The effect of changing the departure time by  $\Delta t_d$  can be seen in Fig. 4.1, which ignores the effects of eccentricity and inclination differences for simplicity.

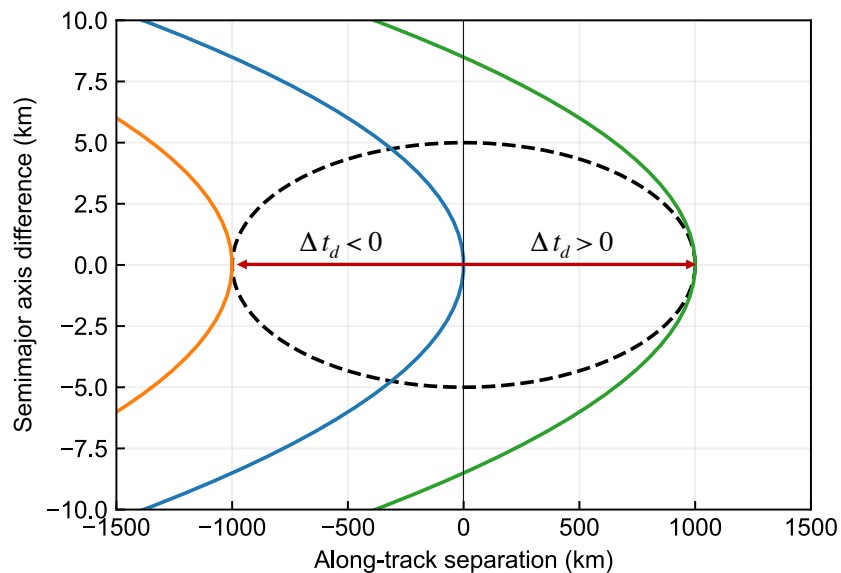


**Figure 4.1:** Examples of the effect on the encounter geometry of departing earlier ( $\Delta t_d < 0$ ) and later ( $\Delta t_d > 0$ ) than the time-optimal take-off time.

The change in take-off time required to move the relative trajectories by a given  $\Delta\psi$  can be approximated from Eq. (3.2.4):

$$\Delta t_d \approx \frac{\Delta\psi}{\dot{\theta}_p - \dot{\theta}_2} \tag{4.1.1}$$

Using the reference orbital parameters, it takes approximately one hour of  $\Delta t_d$  per degree of  $\Delta\psi$ . Since the keepout ellipsoid spans  $17^\circ$  in  $\psi$ , it can take up to 17 hours to push a single trajectory left-wards and deconflict with a space station. When raising a train of multiple satellites that spans several degrees in along-track and deconflicting with more than one station at once, the required  $\Delta t_d$  for deconfliction can be much longer. In particular, departure time offsets of up to one week may be required when considering the worst-case alignment of ISS and Tiangong, which delays arrival to station by about five days. Since it takes another week for Starlink satellites to reach the Tiangong altitude from their parking orbit, deconflicted trajectories must be planned several weeks in advance to allow for early departure times.

Recall from Eq. (2.2.8) that the reference satellite accumulates  $0.72^\circ$  of RAAN error per synodic period at the parking orbit, or  $0.023^\circ/\text{h}$ . Considering a worst-case deconfliction scenario that requires shifting the departure time by one week results in almost  $4^\circ$  of accumulated RAAN error. As discussed in Section 2.3, the RAAN error can be corrected by introducing a waypoint rather than additional cross-track control. When departing early, the waypoint altitude (which defines the along-track rate at the waypoint in Eq. 2.3.4) is set at or above the altitude of the highest space station to eliminate conflicts past the waypoint. When forced to depart late, the reverse-precession altitude is set at a safe distance above the operational target shell.

## 4.2 Prediction Quality and Reactive Re-Planning

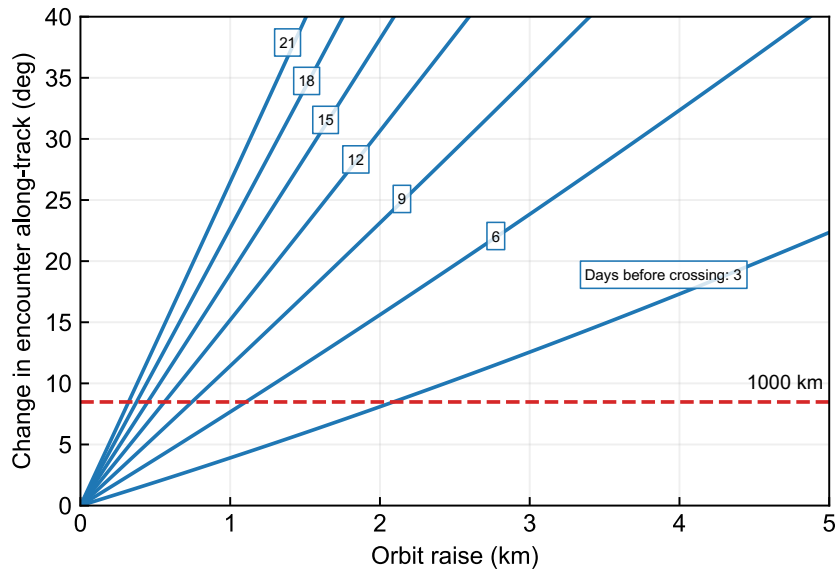
Reference trajectories are planned several weeks prior to the satellites reaching a space station's altitude, which requires long-term predictions of the trajectory of the space station. The accuracy of the departure time offsets and resulting space station close-approach distances are driven by the accuracy of space station trajectory predictions. Unpredicted maneuvers can be particularly impactful.

Figure 4.2 presents an approximate representation of how unpredicted orbit-raising maneuvers executed by a space station change the relative geometry at the time of altitude crossing. The example is based on the reference values in Tables 2.2 and 3.3. For reference, a 1-km orbit-raising maneuver executed one week before the satellite reaches the space station's altitude results in a deviation in excess of 1000 km in the predicted along-track separation, larger than the ellipsoid specified in Eq. (3.1.1). A 2-km raise only three days prior to the encounter yields similar along-track errors.

The later the unpredicted maneuver takes place, the less time there is before take off to set an earlier departure date that deconflicts the trajectories with the space station following Eq. (4.1.1). If there is not enough time to deconflict the trajectories by departing early, the satellites are forced to depart late at the expense of the schedule and propellant costs described in Section 2.3. Large unpredicted maneuvers executed close to the satellites' take-off time or when the satellites are already raising limit SpaceX's ability to re-plan trajectories to stay outside the keepout ellipsoid.

To maximize robustness to unpredicted maneuvers, Starlink's operational screening system is constantly monitoring the reference trajectories relative to the most up-to-date prediction of the stations' trajectories. The system immediately alerts the operators if any of the planned reference trajectories enter the keepout around either space station including wide safety margins. Thanks to constantly screening all planned trajectories, the Starlink operations team can quickly react to any deviations of a space station from its predicted trajectory and re-plan satellite trajectories following Section 4.1 when needed.

The event sequences depicted in Fig. 4.3 compare two scenarios requiring trajectories to be re-planned in response to unpredicted maneuvers of a space station. Figure 3(a) represents a scenario where the



**Figure 4.2:** Effect of unpredicted space station orbit-raising maneuvers on the along-track separation at the time when a satellite reaches the altitude of the space station. The labels indicate how many days before the altitude crossing the maneuver takes place and the red dashed line corresponds to  $T = 1000$  km.

maneuver is detected with enough lead time to plan new trajectories departing earlier than originally planned. Conversely, in the scenario in Fig. 3(b) there is not enough time to avoid the station by departing early.

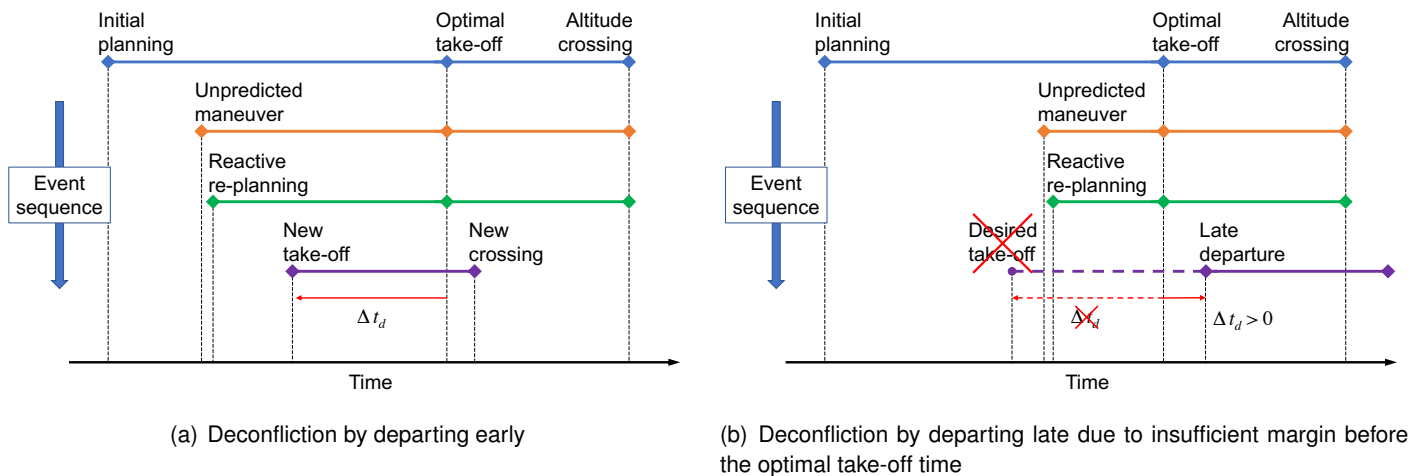


**Figure 4.3:** Event sequence and timeline of two reactive planning scenarios.

SpaceX, having developed a close working relationship with NASA through the commercial resupply services, commercial crew, and other programs, utilizes the same ISS high-precision ephemeris for planning Starlink orbit-transfer trajectories and Dragon mission planning. The ephemeris includes planned maneuvers, minimizing the probability of last-minute operations or opportunity costs in propellant and service-orbit arrival times. SpaceX values NASA’s partnership on this front and encourages similar exchanges of planned burns for operators of all maneuverable spacecraft, not just space stations.

## 5 Conclusions

SpaceX designs the Starlink satellites' orbit-raising and orbit-lowering reference trajectories with a time-optimal path-planning algorithm. The algorithm includes additional constraints to ensure that the Starlink satellites always remain at a large and safe distance from the ISS and Tiangong under nominal circumstances. As an additional safety measure, Starlink's screening system constantly monitors the satellites' planned reference trajectories against the space stations'. The system alerts the Starlink operators immediately when a potential conjunction is detected and reference trajectories are re-planned to change the geometry of the encounter and avoid the conjunction, whenever possible.

SpaceX makes every effort to maintain Starlink's trajectories free of potential conjunctions with the ISS and Tiangong, and will take a similar approach for other crewed stations. The effectiveness of the strategy described in this memorandum is predicated on the availability of accurate predictions of the orbital evolution of stations, particularly those that include planned maneuvers. Otherwise, large uncertainties affect not only SpaceX's ability to accurately screen the trajectories but also its ability to re-plan Starlink trajectories in response to changes in the predicted states. SpaceX strongly endorses the concept that safe operations in space can only be assured with open sharing of maneuver plans and high precision ephemeris between all operators.

The avoidance strategy described in this memorandum covers nominal operation of both the Starlink satellites and crewed space stations. It further assumes that the space stations' ephemeris are known to the Starlink team with sufficient lead time and accuracy. As such, this process does not necessarily provide large clearances to crewed space stations in the event of a non-maneuverable Starlink satellite; a space station failing to follow its published trajectory due to a burn failure or new burn planned with insufficient notice; or a Starlink satellite failing to follow its planned trajectory. Other exceptions apply.

In these scenarios, there is no substitute for real-time dialog between the two spacecraft operators. Starlink operators are available 24-7 for conjunction coordination. Contact information to interface with the Starlink operations team can be found on Space-Track.org, associated with all Starlink satellites.

## References

- 18th Space Control Squadron (2020). Spaceflight safety handbook for satellite operators. Version 1.5, U.S. Space Force, 18 SPCS Processes for On-Orbit Conjunction Assessment & Collision Avoidance.
- Battin, R. H. (1999). *An Introduction to the Mathematics and Methods of Astrodynamics*. AIAA Education Series, Reston, VA.
- Brouwer, D. (1959). Solution of the problem of artificial satellite theory without drag. *The Astronomical Journal* 64(1274), 378–396. DOI: 10.1086/107958
- Coffey, S. L., A. Deprit, and E. Deprit (1994). Frozen orbits for satellites close to an Earth-like planet. *Celestial Mechanics and Dynamical Astronomy* 1(59), 37–72. DOI: 10.1007/BF00691970
- Lara, M. (2015). Efficient formulation of the periodic corrections in Brouwer's gravity solution. *Mathematical Problems in Engineering*. DOI: 10.1155/2015/980652
- Vallado, D. A. (1997). *Fundamentals of Astrodynamics and Applications*, 4th edition. Microcosm Press, Hawthorne, CA.